PAPER

A model of defect cluster creation in fragmented cascades in metals based on morphological analysis

View the article online for updates and enhancements.

IOP **ebooks**™

Bringing you innovative digital publishing with leading voices to create your essential collection of books in STEM research.

Start exploring the collection - download the first chapter of every title for free.

A model of defect cluster creation in fragmented cascades in metals based on morphological analysis

A De Backer[1] , C Domain[2], C S Becquart[3], L Luneville[4,5], D Simeone[5,6], A E Sand[7] and K Nordlund[7]

[1] CCFE—Culham Centre for Fusion Energy, Abingdon, Oxon OX14 3DB, United Kingdom
[2] EDF Lab Les Renardières, Dpt MMC, F-77250 Moret sur Loing, France
[3] Université Lille, CNRS, INRA, ENSCL, UMR 8207, UMET, Unité Matériaux et Transformations, F-59000 Lille, France
[4] CEA/DANS/DMN/SERMA/LLPR-LRC CARMEN, CEA Saclay F-91191 Gif sur Yvette, France
[5] Centralesupelec/SPMS/LRC CARMEN, F-92292 Chatenay Malabry, France
[6] CEA/DANS/DMN/SRMA/LA2M-LRC CARMEN, CEA Saclay F-91191 Gif sur Yvette, France
[7] Department of Physics, University of Helsinki, PO Box 43, FI-00014 Helsinki, Finland

E-mail: andree.de.backer@ukaea.uk

Abstract

The impacts of ions and neutrons in metals cause cascades of atomic collisions that expand and shrink, leaving microstructure defect debris, i.e. interstitial or vacancy clusters or loops of different sizes. In De Backer *et al* (2016 *Europhys. Lett.* **115** 26001), we described a method to detect the first morphological transition, i.e. the cascade fragmentation in subcascades, and a model of primary damage combining the binary collision approximation and molecular dynamics (MD). In this paper including W, Fe, Be, Zr and 20 other metals, we demonstrate that the fragmentation energy increases with the atomic number and decreases with the atomic density following a unique power law. Above the fragmentation energy, the cascade morphology can be characterized by the cross pair correlation functions of the multitype point pattern formed by the subcascades. We derive the numbers of pairs of subcascades and observed that they follow broken power laws. The energy where the power law breaks indicates the second morphological transition when cascades are formed by branches decorated by chaplets of small subcascades. The subcascade interaction is introduced in our model of primary damage by adding pairwise terms. Using statistics obtained on hundreds of MD cascades in Fe, we demonstrate that the interaction of subcascades increases the proportion of large clusters in the damage created by high energy cascades. Finally, we predict the primary damage of 500 keV Fe ion in Fe and obtain cluster size distributions when large statistics of MD cascades are not feasible.

Keywords: irradiation damage, microstructure, defect, vacancy, SIA, loop, subcascade

(Some figures may appear in colour only in the online journal)

1. Introduction

In fission and fusion nuclear installations, structural materials are exposed to non-homogeneous ion and or neutron fluxes. One challenging task pursued for more than 60 years [1] is the characterization of the primary damage, i.e. the defects of the microstructure created by the displacement cascades of energy varying from a few tens of eV to MeV in metals including Fe, Zr, W, Be and alloys. It is established that the number, the type and the size distribution of the defects

depend on the material and the particle energy [2]. The primary damage is the source term of long time evolution model and the large defects are crucial as they can be immobile and stable [3]. In the frame of the multiscale modelling, numerous approaches are pursued such as molecular dynamics (MD) and the binary collision approximation (BCA). The rationalization of the results is essential to the development of large scale models suitable to the study of the spatial inhomogeneity and different neutron spectrum in the nuclear installations [4, 5].

The works reported in [6–11] have showed that cascades can split in subcascades at high energy and that the fragmentation threshold energy depends on the materials. These studies covered a large range of atomic numbers, atomic densities, displacement threshold energies and several crystal structures. Furthermore, they raised the question of the overlap or the vicinity of subcascades and their possible interaction. Interestingly, the formation of large clusters at interfaces between subcascades has been observed in MD cascades in Fe and explained by shock-wave interaction in [12, 13]. The fragmentation of high energy cascades in alloys has been studied using MD thanks to a new approach to reduce the computational time, implemented in the cell molecular dynamics for Cascade code [14, 15]. In [16], the same authors analysed how large clusters influence the output of large scale models like the rate equation cluster dynamics.

In [11, 17], we demonstrated the fractal nature of cascades in the frame of the BCA which naturally introduces power laws in the total number of defects. In [18, 19], we showed the existence of a power law in the frequency of defect clusters as a function of their size in W and in Fe. Recently [20], we proposed a new method of decomposition of cascades in subcascades and a model of defect cluster production of primary knocked-on atoms (PKA) of any energy. The frequency of defect clusters in individual subcascades is multiplied by the frequency of these subcascades in the large fragmented cascades. The interest of our approach is that the subcascade frequency can be efficiently calculated using the BCA and that full MD cascade calculations are only necessary up to the fragmentation energy. In [21] we explains the deviation from the power law of the number of loops per ion as a function of the loop size, observed in experiments of 150 keV self irradiation of W at cryogenic temperature [22].

In this work, we extend our cascade decomposition study to other metals and to MD cascades. Afterwards, cascades are seen as random multitype point patterns formed by the subcascades, the type of which is given by their volume. Using the cross pair correlation functions, we derive the number of interacting subcascades that we include in our model of primary damage. Our model is adjusted on MD cascades and extrapolated to high energy cascades that are hardly accessible to MD.

In the first section we describe the computational methods of simulation of the BCA and MD cascades. I the second section we analyse the subcascade decomposition of BCA and MD cascades and we discuss the choice of the two parameters, i.e. the cell size and the energy criterion E_c. In the third section, using BCA cascades in various metals, we demonstrate

that with the strictest criterion $E_c = 0$, the fragmentation energy follows a simple power law of the atomic number and the atomic density. Then we study the case $E_c \neq 0$, proposing a simple formula based on thermodynamic properties and show that it reduces the fragmentation energy of high melting point metals, particularly high Z ones like W where cascades are very compact. In the fourth section we describe the morphological evolution of cascades taken as multitype point patterns. Each subcascade is one point and its type is its volume. The cascade morphology is captured using the cross pair correlation functions. The pairs are formed by subcascades of different volume. Pairs at close distance from each other are interesting as they are likely to interact. We calculate the numbers of interacting subcascades of different size as a function of the PKA energy and show that they follow broken power laws. This reveals the second morphological transition from fragmentation to branching. In the last section, we develop our model of primary damage for high energy cascades. Our model sums the defect production in individual subcascades and the pairwise terms of the subcascade interactions. The model is adjusted on full MD cascades in Fe from 1 keV to 120 keV. We demonstrate that our model can predict the creation of large SIA clusters due to the subcascade interaction. We finally apply our model to the prediction of the interstitial cluster distribution in the primary damage of high energy cascades, like 500 keV Fe self implantation performed in our TriCEM project, which is not feasible using full MD so far.

2. Computational methods of BCA and MD cascades

BCA cascades are calculated using SDTrimSP [23], the slowing down of the projectile is modelled as described in [24] with no consideration of crystal structure by a series of random collisions and a continuous interaction with electrons. No free surface is included. The Ziegler–Biersack–Littmark (ZBL) potential [25, 26] is used along with the electronic stopping power description of Oen and Robinson [27]. Notice that in [28, 29], the authors demonstrated that the electronic stopping power and the electron-phonon coupling in high energy cascades have little effect on the damage at long times in Fe but reduce the damage in W. Our model cannot take into account these mechanisms. The main material parameters are the atomic number and atomic density. We observed that the threshold displacement energy and other parameters of the BCA model are not significant in this study because they modify the cascade features at smaller space scales than the cubic cell size used in our decomposition method.

For this work, we used MD cascades in Fe described in [30] using DYMOKA [31] with the embedded atom model potential of Ackland *et al* [32] hardened with ZBL [25]. We characterized the validity of this potential to model atomic collisions in the range of the threshold displacement energy by comparison with *ab initio* MD in [33]. Here, classical MD simulations have been performed within the NVE ensemble with periodic boundary conditions with up to 5 488 000 atoms (box of $140 \times 140 \times 140$ cubic cells). After a thermalisation

stage of 3 ps at 100 K, the kinetic energy is given to the PKA. The time step is adjusted during the simulation which lasts 20 ps and no electronic loss is considered. Large statistics have been obtained with several hundreds of cascades per energy up to 120 keV (800–1000 cascades in most of the cases). Half of the cascades were initiated with a $\langle 135 \rangle$ PKA direction and half with a random direction. No statistical difference is observed between both sets. To detect vacancies and SIA defects at the end of the simulation, lattice site analysis is performed. A cluster is defined by all entities (vacancy and SIA) within a critical distance, here equal to the lattice parameter, e.g. second nearest neighbour distance, and the net defect sum determines the cluster size which is used for the statistics of defect clusters.

3. Cascade fragmentation

In our decomposition method, the energy losses at the end of the BCA cascade are projected and averaged on a cubic tessellation of space. The energy density exhibits fluctuations with hot cores separated by low energy interfaces. A criterion of minimum energy density, E_c, distinguishes what is part of the cascade or not and indicates the interfaces between subcascades. The level of details of the cascade morphology is adjusted by the size of the cubic cells of the space tessellation and the energy criterion. The subcascades are determined by coalescence of neighbouring cells. The presence of an interface between subcascades means that it exists a contiguous volume with a thickness of at least one cell where the energy is smaller than E_c. As opposed to other methods based on the tracking of high energy knock-on atoms, we developed an effective decomposition method, i.e. no subcascade overlap is possible. However we will study their vicinity. Figure 1 shows a picture of one 100 keV BCA Fe cascade analysed with different cell sizes and the average number of subcascades as a function of the cell size for different PKA energies (using $E_c = 44$ eV nm^{-3}). One sees a plateau for cell sizes of 1–2.5 nm. This suggests an optimum of the cell size around 1 nm that will be used for the results of the next sections. Small cells lead to a description of the cascade at the level of the collisions. As the energy is averaged on the cell volume, large cells exclude cascade regions of low energy density. One sees that our decomposition method is a coarse-grained approach and the cell size varies the granularity level of the cascade.

We applied the same space tessellation and energy procedure to MD cascades, recording the kinetic energy of the atoms with kinetic energy larger that 0.4 eV. With MD cascades, the subcascade decomposition depends on time. After the ballistic stage, the cascade cools down and no more hot region is detected. The average volumes of 20 keV Fe cascades as a function of time using BCA and MD with various cell size and E_c are plotted in figure 2(a). During the ballistic phase that lasts around 0.1 ps, the volume of BCA and MD cascades increases linearly with a rate that is mainly affected by the cell size for the BCA and E_c for MD. The smaller the cell size, the larger the volume. This is explained by the fractal feature of the BCA cascades. In MD cascades, the collective

interactions between atoms of low kinetic energy make our method more sensitive to E_c in the region surrounding the hot cores (see sketch drawn in figure 2(b)). More description of the thermal processes in MD is out the scope of this paper. With large E_c, only the hottest cores are detected and the total volume is small. With small E_c, subcascades are not distinguished. In the next section we will study both cases, i.e. $E_c = 0$ and $E_c \neq 0$. It remains that after the ballistic stage, the BCA cascades do not evolve any more when the MD cascade volume decreases because of the cooling down. The decomposition method is applied when the volume is maximum, the time of which depends mainly on the PKA energy.

The cascade fragmentation is a stochastic process which depends on the cascade energy. In [20], we described the subcascade volume distribution as a function of the energy. We showed that the distribution is a peak at low energy and turns into a power law at high energy. More precisely, the average number of subcascades as well as the standard deviation depend on the energy. The subcascade formation in Fe has been studied calculating 1500 BCA cascades and several hundreds MD cascades per energy from 1 keV to 2 MeV and 1 keV to 120 keV resp. The frequency of cascades fragmented in subcascades as a function of the energy is illustrated in figure 3(a) as violin plots (the thickness of the green area is proportional to the frequency). One sees that the standard deviation is very small at low energy, increases around the fragmentation energy and trends to saturate at high energy. In figure 3(a), red points are the average number of subcascades, $n_{SC}(E)$, which starts at one as there is one main volume, then becomes progressively proportional to the PKA energy. The first transition corresponds to the fragmentation energy, E_{fr}, that can be determined by fitting with the function

$$n_{SC}(E) = \begin{cases} 1 & \text{if } E \leqslant E_{fr} \\ E/E_{fr} & \text{if } E > E_{fr} \end{cases}. \tag{1}$$

In figure 3(b), we plot the number of subcascades as a function of the PKA energy using MD and BCA cascades and different values of E_c and cell size. The fragmentation energy depends slightly on the cell size and E_c. Both MD and BCA predict that the fragmentation starts between 10 and 15 keV. Notice that without the high level of statistics, for example from a limited number of MD simulations, the point where the number of subcascades equals 2 could be seen as the threshold for subcascade splitting, and our results are in agreement with Stoller's paper [34], which gives the threshold for splitting in Fe as 20–30 keV. The progressive increase of the number of subcascades is due to the averaging and the increase of the probability of small subcascades that decorate the main volume. Notice that the subcascade frequency vanishes for a volume close to the volume corresponding to the fragmentation energy (a thorough description is given in [20]). We determined that in Fe, $E_{fr} = 15$ keV and $V_{fr} = 90$ nm^3.

4. Fragmentation energy within the periodic table

In this section, we will use both $E_c = 0$ and a simple expression for $E \neq 0$. We want to capture correlations between the
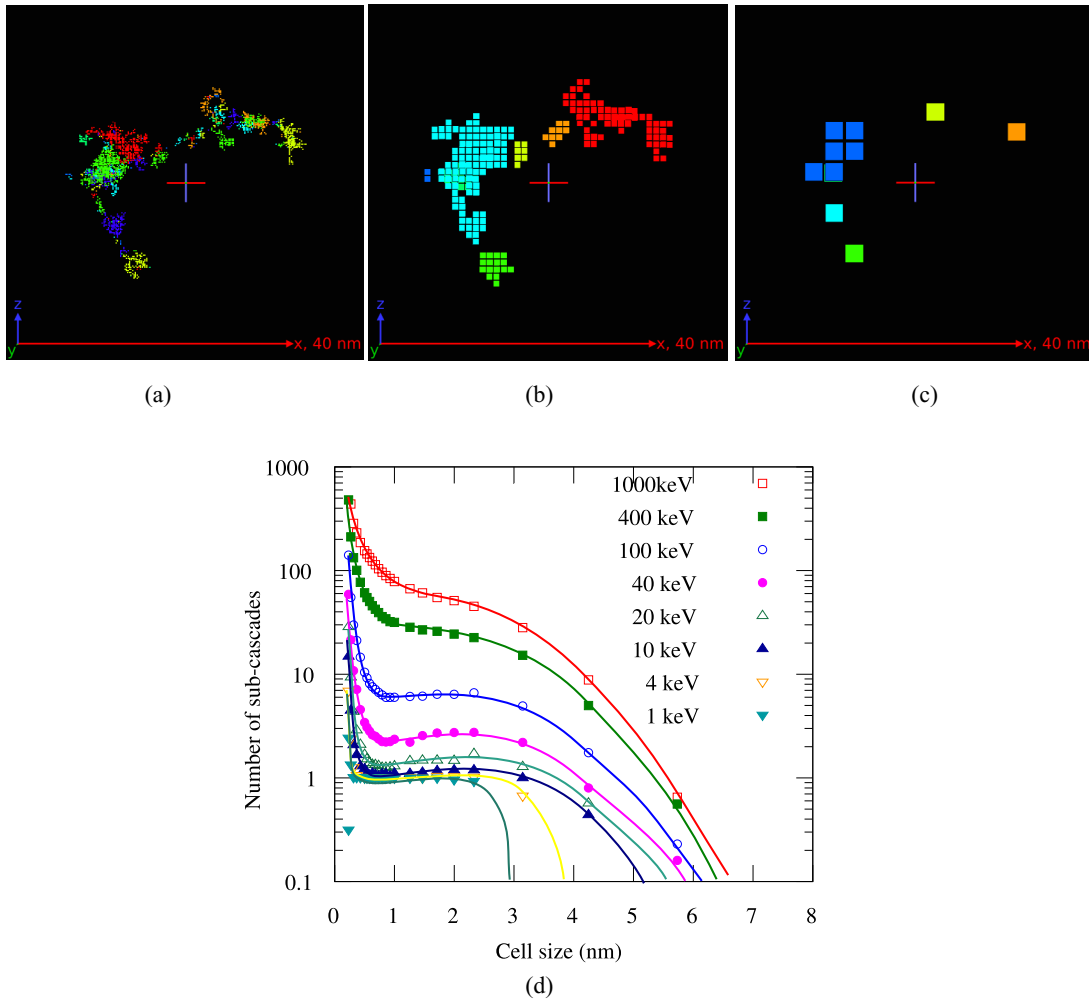
(a)

(b)

(c)

(d)

Figure 1. ((a)–(c)) Pictures of one 100 keV BCA cascade in Fe analysed with increasing cell sizes, 0.2 nm, 1 nm and 3 nm. (d) Average number of subcascades as a function of the cell size and the PKA energy in Fe.
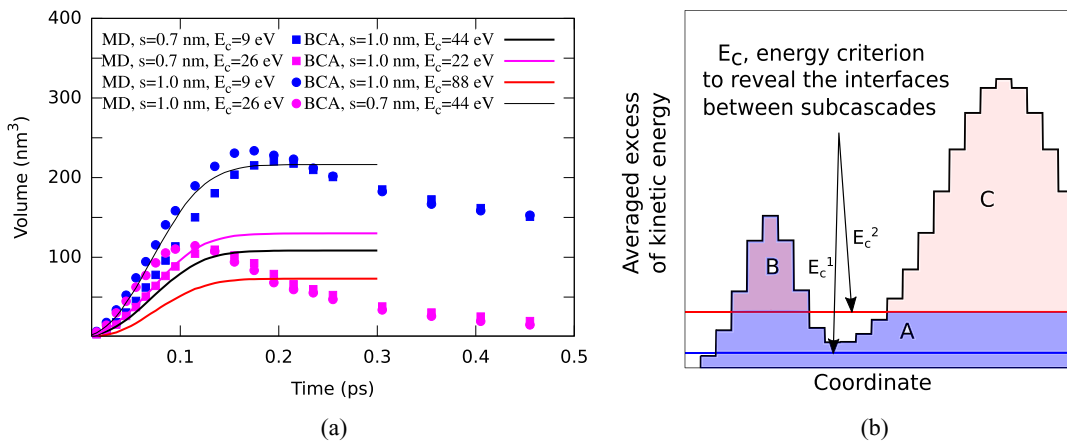

(a)

(b)

Figure 2. (a) Cascade volume as function of time for 20 keV cascades calculated with BCA and MD cascades similarly analysed with various cell sizes, *s* and E_c. (b) Sketch of the effect of E_c which reveals the interface between subcascades: with the small E_c^1, only one subcascade A is detected, with the larger value E_c^2, two subcascades B and C are detected and with a too large value, the volume of small subcascades would be missed.
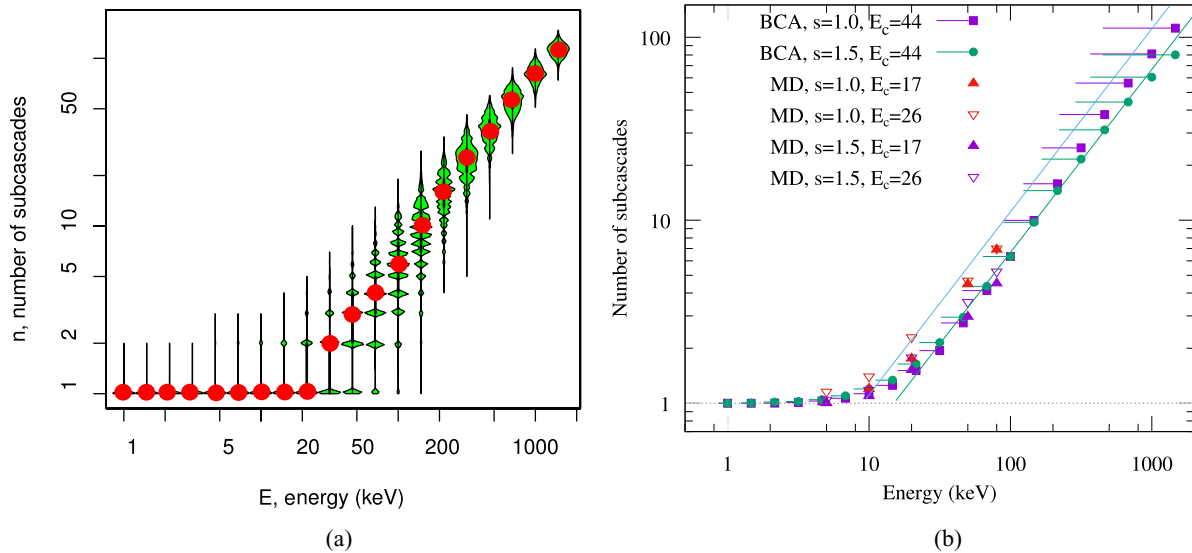
Figure 3. (a) Violin plots of the number of subcascades as a function of the energy with 1500 cascades per energy (BCA results in Fe with $s = 1$ nm and $E_c = 44$ eV nm^{-3}). E is the cascade energy and n is the number of subcascades. The thickness of the green surfaces in the E direction is proportional to the frequency of cascades fragmented in n subcascades. The red points are the average number of subcascades per cascade. (b) Average number of subcascades obtained by MD and BCA as a function of the energy for various combination of the cell size s (in nm) and the energy criterion E_c (in eV nm^{-3}), in Fe. The fragmentation energy obtained by fitting on equation (1) is between 10 keV and 15 keV. Notice that the electronic losses have been included in the BCA model and not in the MD one. Small horizontal bars indicate the energy shift when the electronic losses are removed and it improves the agreement between MD and BCA.

density of energy required to create a hot subcascade core and the properties of the material, applicable to many metals. In [20] we proposed

$$E_c = (C(T_f - T) + L) \quad (2)$$

where C and L are the specific heat and the enthalpy of fusion respectively, T_f and T are the melting point and the material temperature.

The justification is that the melting of the crystal is observed in the hot cores of the cascades and that the formula (2) is a convenient estimate of the energy required to melt the material. The exact amount of energy required to melt a nano-metric cubic cell of material is a complex question. In particular, displacement cascades are not equilibrium processes. The mechanical (superheating) melting temperature is about 15%–20% larger than the melting temperature and the crystal melts immediately with no enthalpy of fusion [35–38]. Furthermore as the specific heat does evolve with temperature, an integral form is more precise. Following [39], one sees that the proper integration from room temperature to melting temperature leads to a 2 times lower energy compared to our expression. These aspects are out of the scope of our paper.

With our simple formula, values of E_c for Be, Fe, Zr, Mo and W are given in table 1. W and Mo require the largest values of 77 eV and 66 eV because of their high melting point and Zr has the lowest value because of its low atomic density. Be has a low melting point but this is compensated by its high atomic density.

BCA cascades were done in 22 metals with PKA energy ranging from 1 keV to 1 MeV. 200 cascades per energy was a sufficient statistics. All metals present a first morphological transition from one single domain to an increasing number of subcascades. The fragmentation energy is obtained by

Table 1. Atomic number, atomic density, energy criterion for 1 nm cells (E_c), maximum fragmentation energy (E_{fr}^{max}, with $E_c = 0$) and the fragmentation energy with $E_c > 0$ given by equation (2).

	Atomic number	Atomic density (atom per nm^{-3})	E_c (eV nm^{-3})	E_{fr}^{max} (keV)	E_{fr} (keV)
Be	4	123	37	0.75	1.1
Al	13	60	11	4	1.8
Fe	26	85	44	45	15
Ni	28	91	51	58	21
Zr	40	43	30	20	9
Mo	42	65	66	84	17
W	74	63	77	315	75[a]

[a] This value is smaller than the one in [20] because of the choice of equation (1).

fitting on equation (1). In our study, the parameters differing one material from another are the atomic number, Z, the atomic density, d and the properties included in the energy criterion, E_c.

We first described the effect of the atomic number and the atomic density by repeating the BCA cascade decomposition taking $E_c = 0$. In this case, the criterion is the strictest and the fragmentation energies are maximum. The atomic number varies from 4 for Be, to 92 for U and increases the fragmentation energy. The atomic density varies from 43 at. per nm^3 for Zr to 123 at. per nm^3 for Be and also increases the fragmentation energy. Interestingly, the density of metals (after Be which has only 2s electrons per atom) evolves as three successive bell shape curves with the filling of the successive electronic bands 3d, 4d and 5d as explained in [40]. Because of the effect of the atomic density, the bell shapes is also observed on the fragmentation energy when one sweeps along the periods of the periodic table (with $E_c = 0$).
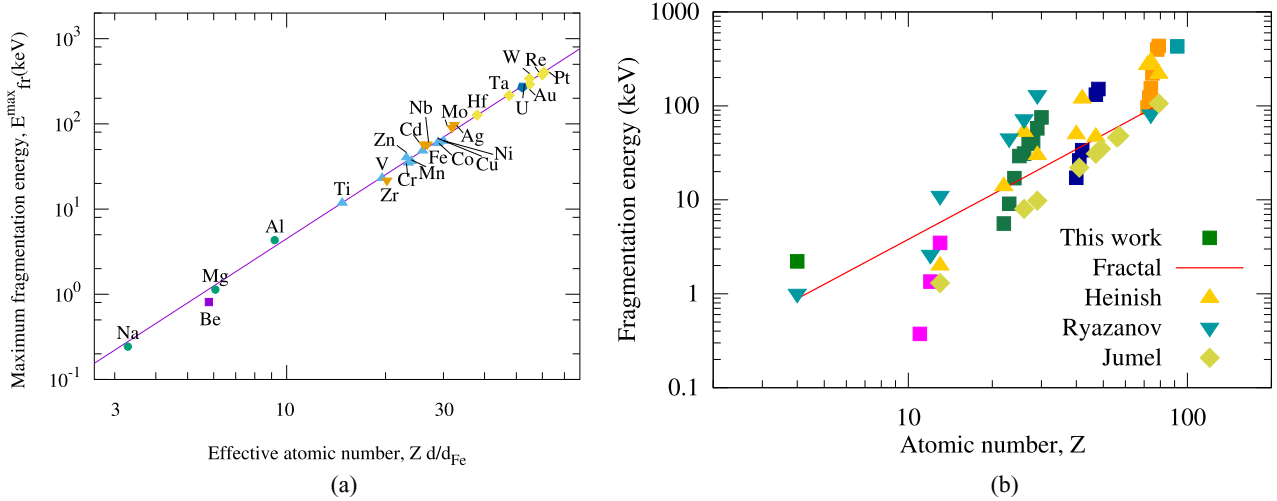
Figure 4. (a) Fragmentation energy as a function of the effective atomic number equal to Zd/d_{Fe} where, Z is the atomic number and d is the atomic density (d_{Fe} being the atomic density of Fe), with $E_c = 0$. The line corresponds to the power law given by equation (3). (b) Fragmentation energy as a function of the atomic number, with $E_c > 0$ and given by the formula (2), compared to our fractal approach [41], the self consistent theory of Ryazanov [10], the break-up energy reported by Heinisch [8] and the analytic model of INCAS reported by Jumel [9]. Our results do not follow a simple power law of Z because of the effect of the atomic density and the energy criterion. These results have been obtained with BCA cascades.

In our previous work [41], we demonstrated that the fragmentation energy follows a power law as function of the atomic number when the density is constant. Using this new approach which easily includes the effect of the atomic density, we found that the fragmentation energy follows a power law,

$$E_{fr}^{max} = E_1 \left(Z \frac{d}{d_{Fe}} \right)^{q_c} \qquad (3)$$

function of an effective atomic number defined by $Z d/d_{Fe}$, where Z is the atomic number and d is the atomic density (with Fe as reference material). Our results and this expression using $E_1 = 0.013$ keV and $q_c = 2.5$ are plotted in figure 4(a). Notice that the maximum fragmentation energy is large, 45 keV for Fe and 315 keV for W for example. The reason is that $E_c = 0$ is too strict: it requires that no cascade related event occurs in an interface of 1 nm thick to identify two distinct subcascades.

The fragmentation energy with $E_c > 0$ is plotted in figure 4(b). It varies between 2 keV and 500 keV depending on the metal and follows a sawtooth evolution as a function of the atomic number of metals of groups 2s, 3p, 3d, 4d, 5d and now E_c. The decrease of the density is compensated by a low E_c (due to low melting point) for most metals of the right part of each period, columns 11 and 12 of the periodic table, Cu, Zn, Ag, Cd, Pt and Au. The fragmentation energy is 15 keV for Fe and 75 keV for W, which is in agreement with full MD cascades and experimental results [21]. Notice that this last value is divided by 2 compared to our previous work where the fragmentation energy was defined as the energy where cascades form two subcascades.

In figure 4(b) we also represents the fragmentation energies using the fractal approach [17, 41] and other methods from [8–10]. The general tendency of the effect of the atomic

number is visible. However, in our work and proposing the equation (3), we separated the effect of the atomic density and the atomic number. The main difference between the method of [8] and our is the introduction of E_c which reduces (resp. increases) the number of subcascades for metals with a large E_c, i.e. a high (resp. low) melting temperature or heat capacity for example. Notice that our method is an effective method where no cascade overlap is possible, contrary to [9, 10]. Interestingly Heinish's method using MARLOWE [42] takes into account the crystal structure. The authors noticed that the reduced fragmentation energies group by crystal structure but that study did not separate the effect of the atomic density and the crystal group. Notice that our study does not include the elongated cascades produced by ions which experience channelling due to the periodicity of the lattice. We believe that the effect on the fragmentation energy and the average number of subcascades is limited.

The methods also sometimes differ by the choice of the interaction potential, ZBL and Moliere potentials, the later produces a larger collision cross section at low energy, i.e. should predict more dense cascades and consequently larger fragmentation energy.

With our study of BCA cascades, we characterised, firstly, the evolution of the fragmentation energy with the atomic number, secondly, the evolution of the fragmentation with the atomic density, and thirdly, we have shown how the fragmentation energy may depend on thermodynamic properties. Further works are necessary to fully confirm the effect of the thermodynamic properties and determine the effect of the interatomic potentials.

5. Subcascade spatial correlation

In this section, we further study the cascade morphology and derive the number of pairs of subcascades likely to interact
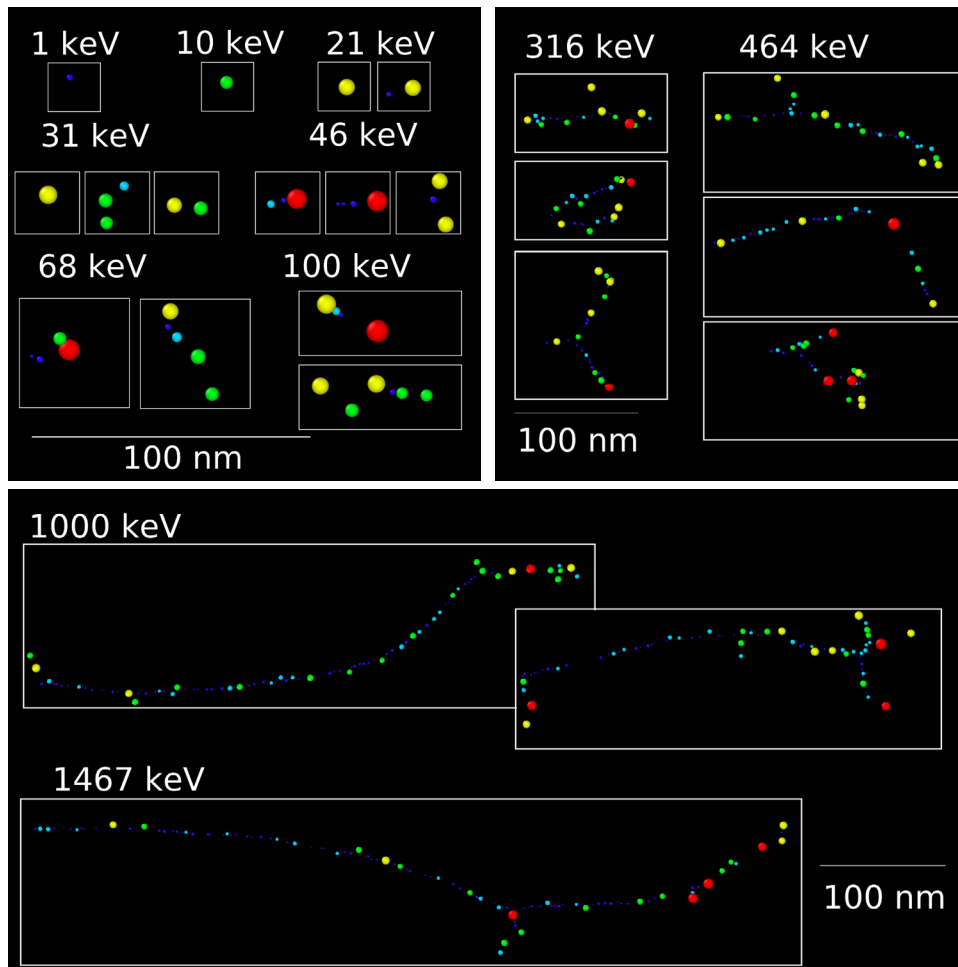
Figure 5. 1 keV–1.4 MeV Fe BCA cascades analysed with our decomposition method. Subcascades are represented by spheres. The colours distinguish 5 different subgroups based on a volume criterion given in table 2. Blue, cyan, green, yellow and red are resp. XS, S, M, L and XL subcascades.

because they are at close distance from each other. In the next section we will propose the resulting correction term of our model of primary damage.

We used BCA cascades from 1 keV to 1.4 MeV, with 1500 cascades per PKA energy in Fe. The centres and volumes of the subcascades form random multitype point patterns. Fe is a particularly interesting metal as the fragmentation energy is relatively low, and both sides of the first transition are covered by the energy range studied here. Fe BCA cascades described as multitype point patterns are illustrated in figure 5. For simplicity, subcascades are divided into 5 subgroups depending on their volume. The subgroups are named XS, S, M, L and XL and are respectively coloured in blue, cyan, green, yellow and red, with the size limit given in table 2. One can describe the growth of the random multitype point patterns as function of the energy as follows. At low energy they consist of one small sphere. When the energy increases, the spheres first grow. Around 15 keV, small decorations start to appear in some patterns. At higher energy, multiple spheres of various size are visible at random distance from each other. Above 100 keV, small spheres align along branches and large ones are found at the intersections or ends of branches.

The cross pair correlation function characterizes the spatial distribution of points composing random multi-type patterns. It is used in other studies of multicomponent systems, like the modelling of the structure of GeO_2 glasses [43, 44], the analysis of atom probe tomography data [45], the study of different species of trees [46] or other examples of spatial point patterns [47, 48]. It quantifies the frequency of objects as a function of their mutual distance and we will use it to count the interacting subcascade number considering a vicinity criterion.

Because of the continuous variation of the subcascade volume, the cross pair correlation function depends on 4 continuous variables, $g(r, v_i, v_j, E)$ where r is the distance between the centres, v_i and v_j are the subcascade volumes and E is the PKA energy. The centre of the subcascade is defined as $\vec{r_i} = \frac{1}{n_i} \sum_{k=1}^{n_i} \vec{\rho_k}$ where $\vec{\rho_k}$ are the positions of the n_i cubic cells forming the subcascade after our decomposition method. One has $v_i = n_i v_{EC}$ where v_{EC} is the volume of the cubic cell equal to $1\,nm^3$.

Instead of continuous variable for v_i and v_j, we used 5 volume subgroups, XS, S, M, L and XL. The cross pair correlation functions can be calculated as

Table 2. Description of the subcascades distributed in 5 subgroups of different volume, XS, S, M, L, XL. Radius and PKA energy that can be associated with each group. For 500 keV Fe cascades, average n_i^k (number of subcascades of group i per cascade) and $N_{i,j}$, average numbers of interaction of subcascades for all cross pairs, XS–XS, XS–S, ..., XL–XL (see equation (8)).

i or j	XS	S	M	L	XL
Volume (nm³)	0–10	10–40	40–90	90–180	180–1500
R_i (nm)	1.1	1.7	2.5	3.5	5
Energy (keV)	1	5	10	20	50
for $E = 500$ keV					
average n_i^k	19	8	5	3	2
$N_{XS,j}$	0.51	1.0	0.09	0.11	0.025
$N_{S,j}$		0.027	0.067	0.013	0.044
$N_{M,j}$			0.006	0.057	0.01
$N_{L,j}$				0.014	0.003
$N_{XL,j}$					0.012

$$G_{i,j}(r,E) = \frac{1}{4\pi r^2 dr} \frac{1}{n_c}$$
$$\times \sum_{k=1}^{n_c} \left(\frac{1}{n_{i,k} n_{j,k}} \sum_{i'=1}^{n_{i,k}} \sum_{j'=1}^{n_{j,k}} H(|\vec{r_{i'}} - \vec{r_{j'}}| - r) H(r + dr - |\vec{r_{i'}} - \vec{r_{j'}}|) \right)$$
$$(4)$$

where i and j can be XS, S, M, L or XL, r is the distance between subcascades, dr is the bin width of r, $n_{i,k}$ is the number of points in subgroup i in the cascade k, $H(x)$ is the Heaviside step function and n_c is the number of cascades.

First the contributions of the 5 subgroups to the average number of subcascades and the cascade volume as a function of the PKA energy were calculated (see figure 6). At low energy, the average number of subcascades is one, successively of XS and S type. At the first transition when the number of subcascades becomes larger than one, M and L subcascade types appear associated with subcascades of XS and S type. Above the fragmentation energy, the number of subcascades increases linearly with the PKA energy. One sees the large contribution of XS and S subcascades in agreement with what we described in [20]: the subcascade distribution follows a power law of the subcascade volume for PKA energies above the fragmentation energy.

The total cascade volume and the different contributions are plotted in figure 6(b). At low energy, one type of subcascade, successively of XS, S, M and L type, mainly contributes to the cascade volume. Above around three times the fragmentation energy ($\simeq 50$ keV), all categories contribute to the total volume, however the L and XL subcascades contribute the most.

We analysed the 15 cross pair correlation functions for each PKA energy. Figure 7 shows only the cross pair correlation functions of the 500 keV cascades in Fe. They exhibit a maximum as function of r. The position of this maximum depends on the i,j pair. The main reason is that our decomposition method excludes the possibility of overlap which imposes a minimum distance between subcascades. On the other side, the whole cascade is enclosed in a limited volume then the

pair correlation function vanishes when r increases. Notice that $G_{XS,L}(r,E)$ is not negligible at short distance because the shape of a large subcascade is not spherical and there is a probability that one XS subcascade is almost enclosed in a large one. The position of the maximum roughly increases with the subcascade volume, for example 3 nm for XS–XS subcascades and 6 nm for the S–S subcascades.

When the number of subcascades per PKA becomes larger than 2, the subcascade interaction is possible. For $n_{SC}(E)$ subcascades, the number of pairs is simply $\frac{1}{2} n_{SC}(E)(n_{SC}(E) - 1)$. As the number of subcascades is almost proportional to the energy (see equation (1)), the total number of interacting subcascades is

$$N^{tot}(E) = \frac{1}{2} \frac{E}{E_{fr}} \left(\frac{E}{E_{fr}} - 1 \right) \propto E^2 \quad (5)$$

which is approximately proportional to the square of the energy but does not detail the type of subcascades, and does not take into account their mutual distance. It is reasonable to consider that only subcascades close to each other will interact. The frequency of interacting subcascades is then reduced to integration of the cross pair correlation function on a limited distance interval. We propose a simple estimate of the number of interacting subcascades of volume v_i and v_j in cascades of energy E, equal to

$$N_{i,j}(r,E) = 4\pi r^2 G_{i,j}(r,E) n_i(E) n_j(E) \Delta r \quad (6)$$

where $n_i(E)$ is the average number of subcascades of volume v_i in cascades of energy E and Δr is the distance range where the interaction is significant. We naturally propose to take $r = r_{i,j}^{max}$ where the cross pair correlation functions are close to the maximum and we observed that

$$r_{i,j}^{max} \simeq R_i + R_j + \Delta r$$
$$\text{with } R_i = \left(\frac{3}{4\pi} v_i \right)^{\frac{1}{3}} \quad (7)$$

where R_i is our definition of the subcascade dimension and Δr is 1 nm which is also the size of the cubic cells used in our decomposition method. The number of pairs of effectively interacting subcascades of size i,j is finally

$$N_{i,j}(E) = 4\pi (r_{i,j}^{max})^2 G_{i,j}(r_{i,j}^{max}, E) n_i(E) n_j(E) \Delta r. \quad (8)$$

This simplification will be also justified in the next section, where the effect of the subcascade interaction on the primary damage will be discussed.

Using the equations (5) and (8), we can study the number of interacting subcascades as a function of the PKA energy and the i, j pairs and some of them (XS–S, M–L and XL–XL) are plotted in figure 8. With our estimate, the number of interacting subcascades is several times smaller than the total number, $N^{tot}(E)$. The difference increases with energy because the fragmentation of high energy cascades in a large volume reduces the probability of pairs of subcascades at short distance from each other. Interestingly, the number of XS–S pairs which is an important term of the sum evolves proportionally to E^2 around the fragmentation energy and becomes $\propto E$ at high energy. This is a feature of the cascade branching.
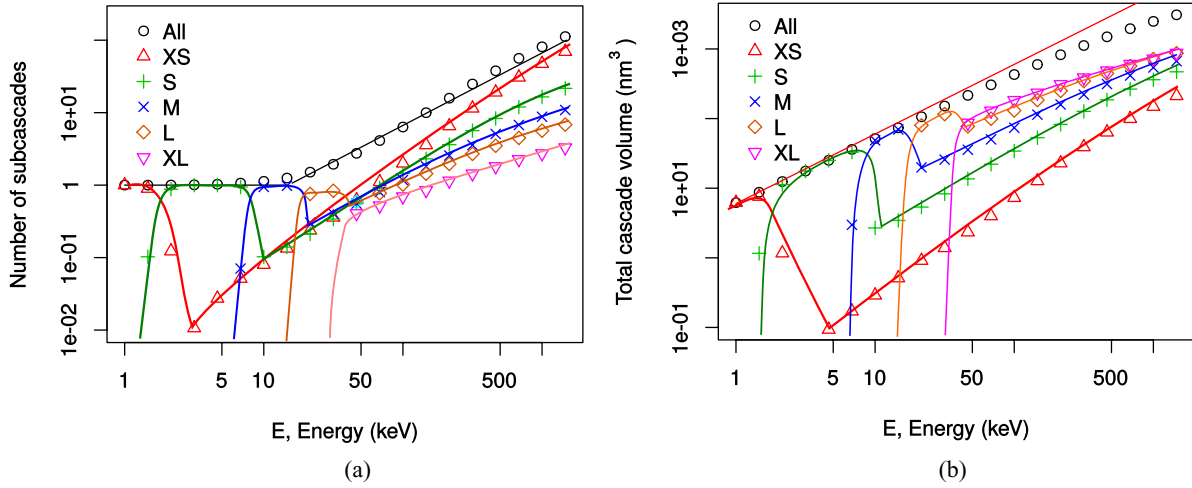
Figure 6. (a) Number of subcascades as function of the PKA energy in the XS, S, M, L and XL subgroups described in table 2. The subcascade subgroups correspond roughly to 1, 5, 10, 20 and 50 keV cascades. (b) Total volume of cascades as function of the PKA energy and the contributions of the XS, S, M, L and XL subcascades. Lines are guides for the eyes. The number of subcascades is proportional to the energy over the fragmentation energy and the cascade volume is proportional to the energy, slightly sub-linear because of the electronic stopping power. BCA cascades have been used for this analysis.
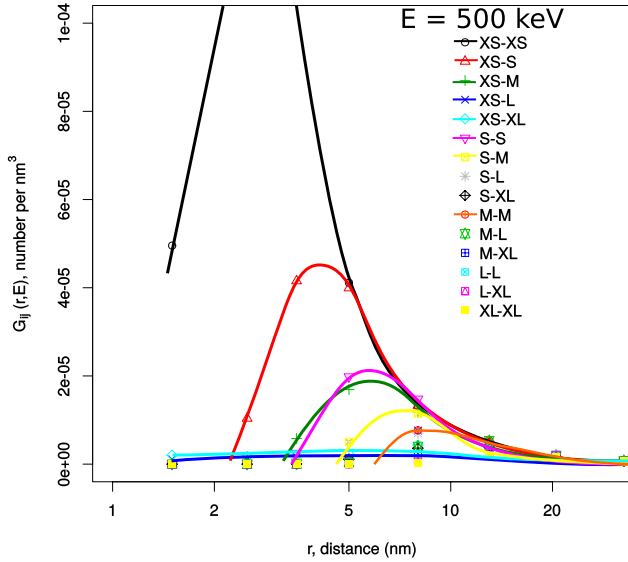

Figure 7. Cross pair correlation functions versus the distance between XS, S, M, L and XL subcascades for $E = 500$ keV and BCA cascades.

Figure 8. Number of XS–S, M–L and XL–XL pairs of interacting subcascades per cascade as a function of the PKA energy calculated with equation (8). Comparison with the maximum number of pairs, N^{tot} (equation (5)). BCA cascades in Fe have been used for these results.

Indeed, the high energy cascades are made of a number of XS and S subcascades $\propto E$ which are found along the branches formed by the fast knock-on atoms (see blue small spheres in figure 5). The number of close pairs is then proportional to E. The number of medium and large interacting subcascades is $\propto E^s$ with s smaller than 1 and equal to 0.5 and 0.25 for M–L and XL–XL. This is due to the sub-linear increase of the number of these subcascades as function of the PKA energy and the reduction of the cross pair correlation function due to the expansion of the cascades in space.

6. Subcascade interaction and primary damage

In the previous section, we studied and characterized the cascade morphological transitions and evolution with the PKA
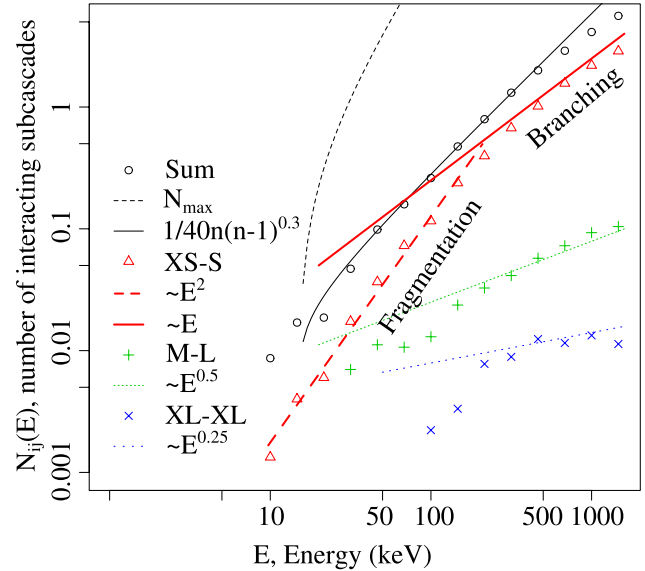
energy using our subcascade decomposition method. We proposed a simple expression of the number of interacting pairs of subcascades of size i, j. We now include the subcascade interaction in our model of the primary damage.

Firstly the key features of the evolution of cascade morphology with energy will be described. Secondly, they are included in our model of point defect and defect cluster production. Then we will demonstrate the relevance of the subcascade interaction and adjust the model by direct comparison with defect production in high energy cascades in Fe calculated by full MD. Finally, we will predict the defect cluster size distribution at even higher energy when MD cascades are not available.
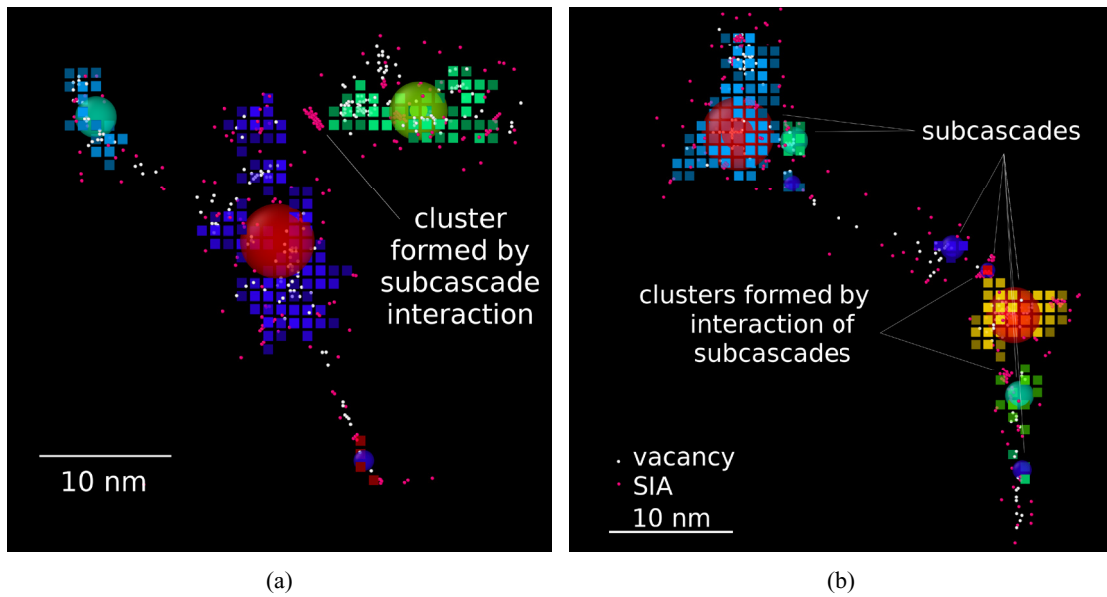
(a)

(b)

Figure 9. Two examples of 80 keV MD cascades in Fe. Our subcascade decomposition method at the maximum expansion of the cascade determined 4 (in (a)) and 8 subcascades (in (b)) illustrated by cubes of different colours. The associated multitype point patterns are schematized by large spheres: blue, cyan, green, yellow and red are resp. XS, S, M, L and XL subcascades. Defects remaining after the cooling of the cascades are superposed as small white for vacancies and magenta spheres for SIAs. Vacancy defects are found mainly in the cores of the subcascades. The SIA defects are found at the periphery of the subcascades. Particularly large SIA clusters are indicated between two L and XL subcascades.

As a premise, figure 9 illustrates two 80 keV MD cascades. The subcascades at the maximum volume expansion (formed by cubes of different colours) are superposed to the large spheres of the multitype point pattern and to the defects remaining at the end of the cascade (small white and pink spheres). One sees the vacancy defects (in white) mainly in the centre of the subcascades. The small SIA defects (magenta) are found around the subcascades. Interestingly, a large SIA loop is found between one L and one XL subcascade.

When the PKA energy increases, the probability of large energy secondary knock-on atoms that create subcascades without overlap becomes possible. This causes the spatial fluctuations of the density of energy used to detect the cascade fragmentation in two or more intense cores of subcascades, separated by interfaces where knocked-on atoms loose no or very few energy. The atoms are ejected from the hot cores to their periphery. Interfaces are thus susceptible of collecting atoms ejected from two different cores. Moreover, shock-waves are emitted by the cascade cores and are likely to interact at interfaces.

The average number of subcascades per cascade is equal to one for small PKA energies and proportional to the energy above the fragmentation energy, E_{fr} (see figure 3). Statistics of subcascades as a function of their volume reveals one aspect of the first morphological transition described in [20]. At low energy, the distribution can be described by a peak around the average volume and a power law of small volumes that represents rare small subcascades decorating the main one. The position of the peak moves toward large volumes when the PKA energy increases. The power law contribution also increases with the PKA energy. Above the first transition, the

peak disappears and only the power law is visible and continues to increase. A deviation to the power law is observed when the frequency of subcascades vanishes, which indicates the maximum subcascade volume, as described in [20, 21]. The maximum subcascade volume slowly increases with the energy up to 2–3 times the fragmentation volume. The total volume of the cascade remains proportional to the PKA energy. The number of subcascades as described in the previous section can be obtained by integration of the distribution. One has

$$V(E) = \int v D(v, E) \mathrm{d}v = V_{\mathrm{fr}} \frac{E}{E_{\mathrm{fr}}}$$
$$n_{\mathrm{SC}}(E) = \int D(v, E) \mathrm{d}v \qquad (9)$$

where $V(E)$ is the total volume, $D(v, E)$ is the distribution of subcascades and V_{fr} and E_{fr} are the fragmentation volume and energy.

In [17], we proposed that the total defect production at any PKA energy, $P(E)$, is the sum of the defect production in individual subcascades. In [20], we extended this approach to the different contributions of clusters of n defects $p(n, E)$. One has

$$P(E) = \int p(n, E) n \, \mathrm{d}n. \qquad (10)$$

At this stage, we do not know if the interaction of subcascades will increase or decrease the number of defects of size n. We introduce the subcascade interaction as pairwise terms and the production of defects of size n becomes

$$p(n, E) = F_1(n, E) + F_2(n, E)$$

$$= \int f_1(n, v) D(v, E) \mathrm{d}v$$

$$+ \int \int \int f_2(n, v_i, v_j, r) S(E, v_i, v_j, r) \mathrm{d}v_i \mathrm{d}v_j \mathrm{d}r \quad (11)$$

where $F_1(n, E)$ is the defect production in individual subcascades and $F_2(n, E)$, the subcascade interaction pairwise terms. $f_1(n, v)$ is the number of defect of size n created by a cascade of volume v, $f_2(n, v_i, v_j, r)$ is the interaction of two cascades of volume v_i and v_j at distance r from each other and $S(E, v_i, v_j, r)$ the average number of pairs of subcascades of volume v_i and v_j at a distance r in cascades of energy E. Subcascades are described in discrete subgroups of volume, XS, S, M, L and XL and in the previous section, we detailed the expression (6) and one sees that

$$S(E, v_i, v_j, r) \simeq N_{i,j}(r, E) \quad (12)$$

where $N_{i,j}(r,E)$ was simplified in $N_{i,j}(E)$ (see equation (8)). Here also, $f_2(n, v_i, v_j, r)$ depends on the distance between subcascades and should also vanish at large distance. This suggests a similar simplification and equation (11) simplifies in

$$p(n, E) \simeq \int f_1(n, v) D(v, E) \mathrm{d}v + \sum_{i,j} f_{2,i,j}(n) N_{i,j}(E)$$

$$\text{with } f_{2,i,j}(n) \simeq f_2(n, v_i, v_j, r_{i,j}^{\max}) \quad (13)$$

where the second term is a sum of the product of the elements of two matrices, the first one gives the interaction of two subcascades of volume i and j at a distance $r_{i,j}^{\max}$, and an example of the second one is given in table 2 for $E = 500$ keV.

Different approaches are surely possible to determine $f_{2,i,j}(n)$ as for example, the overlap study of [49]. For our work, after analysis of the defect production by MD cascades we propose functional forms for $f_1(n, v)$ and $f_{2,i,j}(n)$ with a limited number of parameters. Like in [20, 21], one has

$$f_1(n, v) = \frac{A(v)}{n^S} \left(1 - \frac{n}{n^{\max}(v)} \right)$$

$$\text{with } A(v) = A_{\mathrm{fr}} \left(\frac{v}{V_{\mathrm{fr}}} \right)^T$$

$$\text{and } n^{\max}(v) = n_{\mathrm{fr}}^{\max} \left(\frac{v}{V_{\mathrm{fr}}} \right)^U \quad (14)$$

where S is the exponent of the power law already observed in [18], $n^{\max}(v)$ is the maximum defect size that can be created in a subcascade of volume v and $n_{\mathrm{fr}}^{\max}$ is the maximum cluster size at the fragmentation energy. A convenient functional form for $f_{2,i,j}(n)$ is

$$f_{2,i,j}(n) = \frac{F_{i,j}}{n^\alpha} \left(\delta_{1,n} + \cos \left(\frac{3\pi}{2} \left(\frac{\log(n)}{\log(n_{i,j}^{\max})} \right)^\beta \right) \right)$$

$$F_{i,j} = \gamma \left(\frac{\sqrt{v_i v_j}}{V_{\mathrm{fr}}} \right)^\epsilon$$

$$n_{i,j}^{\max} = \zeta \left(\frac{\sqrt{v_i v_j}}{V_{\mathrm{fr}}} \right)^\kappa \quad (15)$$

Table 3. Parameters of the model of primary damage, $p(n,E)$, that includes two terms: $F_1(n, E)$, the defect production of subcascades taken individually and $F_2(n, E)$, the correction due to the subcascade interaction. Notice that the fragmentation energy and volume have been determined in the first section, $E_{\mathrm{fr}} = 15$ keV and $V_{\mathrm{fr}} = 90$ nm^3.

$F_1(n, E)$		$F_2(n, E)$	
S	2.77	α	2.2
A_{fr}	22	β	1.7
T	0.61	γ	-950
$n_{\mathrm{fr}}^{\max}$	61	ϵ	0.8
U	0.82	ζ	75
		κ	0.9

where $n_{i,j}^{\max}$ is the maximum defect size impacted by the interaction of two subcascades of volume v_i and v_j. The cosine (with the logarithmic argument) leads to a positive and a negative part with a zero at an adjustable defect size equal to $(n_{i,j}^{\max})^{1/3^{1/\beta}}$. $\delta_{1,n}$ is the Kronecker delta and the power law of n is similar to $f_1(n, v)$. In equation (15), we assume that $F_{i,j}$ increases with the subcascade volume because a larger effect is expected from the interaction of a pair of large subcascades than small subcascades. Notice that this functional form is adimensional, symmetric in i and j and determined by 6 parameters, α, β, γ, ϵ, κ and ζ. Also, $f_{2,i,j}(n)$ is independent of E and can be adjusted on the defect production of PKA energy larger than the fragmentation energy.

For this work, we applied our approach using partially the database of MD cascades in Fe from [30]. Further results will be reported separately. Below the fragmentation energy, the defect cluster production follows a simple power law with the expected deviation due to the maximum defect size. At high energy, a hump is visible for the large defects and we see that it cannot be explained by the production of individual subcascades. We adjusted the parameters of $f_1(n, v)$ given by equation (14) on these low energy cascades (from 1 to 10 keV) using Openturns [50]. The 6 parameters of $f_{2,i,j}(n)$ has been adjusted using the 80 keV MD cascades. Because the electronic stopping power is included in our BCA cascades and not in the MD cascades, we use the matrix $N_{i,j}(E)$ of the 100 keV BCA cascades. The parameters are given in table 3.

We are now able to extrapolate our model of primary damage to 500 keV cascades, using the morphological description given by the BCA. Both contributions, i.e. the defect production of subcascades taken individually, and the correction due to the subcascade interaction, have been calculated. In figure 10(a), we plot the defect production calculated with and without subcascade interaction for the 5 keV, 80 keV and 500 keV, and compared to the defect production from the MD cascades. The defect production in 5 keV cascades where the subcascade interaction is insignificant is correctly given by the main term $F_1(n, E)$. For the 80 keV cascades, the subcascade interaction causes a reduction of the frequency of the small defects and a hump of the large defects. In figure 10(b) the functions $f_{2,i,i}(n)$ are plotted.

One sees that they are first negative then positive when n increases, which causes the reduction of the production of
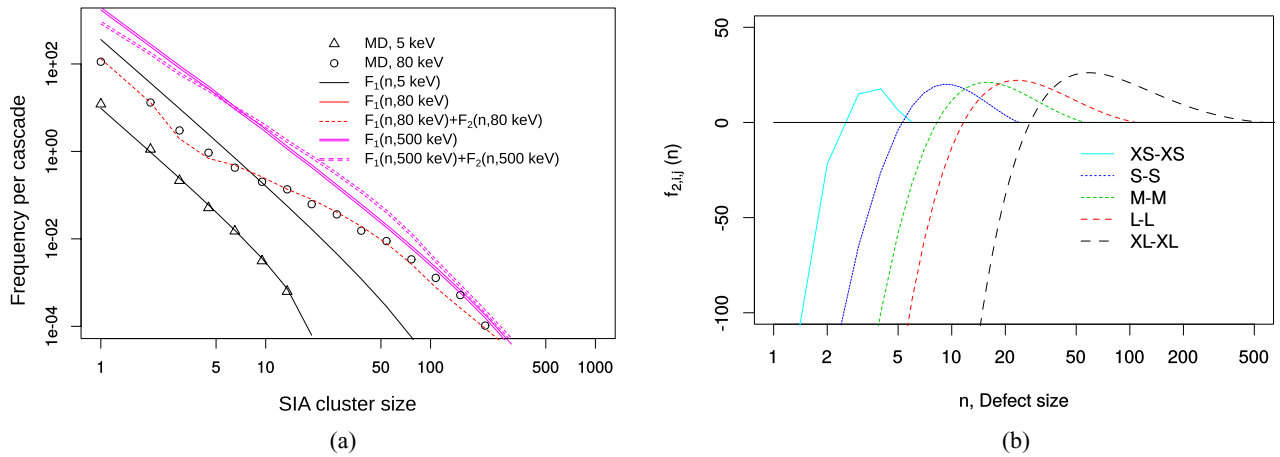
(a)

(b)

Figure 10. (a) The comparison of defect cluster frequencies from MD and our model with and without the subcascade interaction for 5 keV and 80 keV cascades and our model prediction for 500 keV cascades based on the morphology given by the BCA only. The solid and dotted lines have been obtained with our model (equation (11)) that consists in two terms, i.e. the first one counts the defect created in subcascades and the second one is a correction due to the subcascade interaction. The model has been adjusted on the defects created in MD cascades in two steps: F_1 using statistics made on low energy cascades only where subcascade interaction is extremely rare and F_2 using the defects created in large energy cascades where the subcascade interaction is significant. Consequently, F_1 curves fit well the defects of the 5 keV cascades but poorly the 80 keV ones. (b) $f_{2,i,j}(n)$ functions of the subcascade interaction used in (13).

small clusters, and the increase of the production of large clusters when two subcascades interact. The positions of the zero and the maximum cluster size increase with the volume of the interacting subcascades. The consequence is visible on the extrapolation to the primary damage of the 500 keV cascades, where our model predicts an increase of the fraction of clusters due to the subcascade interaction.

7. Discussion

We proposed a systematic method that decomposes any cascade in subcascades with no overlap. We described how two parameters, the cell size and the energy criterion influence the subcascade decomposition. The method has been applied to BCA and MD cascades and it appears that the number of subcascades is independent of the cell size in a wide range of value from 1 nm to 2 nm. With a strict criteria considering no collision in the subcascade interface ($E_c = 0$), we found that the fragmentation energy is a power law of an effective atomic number given by the product of the atomic number and the atomic density, due to the fractal nature of the cascades. To improve the subcascade interface detection, we proposed a less strict criterion, E_c given by a simple formula (2) and applied our method to more than 20 metals. It decreases the fragmentation energy to values which are in agreement with MD and experimental results for W. The fragmentation energy of W is 75 keV with $E_c = 76$ eV nm^{-3} compared to 315 keV with $E_c = 0$. Still these values slightly vary with the cell size and the energy criterion. There is no well-established definition of the threshold energy of cascade fragmentation. With significant statistics, our method demonstrated that this is a stochastic process with a continuous increase of the frequency of small decorations around the main subcascade. Clear features of the subcascade decomposition above the fragmentation energy are the disappearance of any specific subcascade volume and the existence of

a maximum subcascade volume. Indeed, the distribution of subcascade volume turns from a peak to a power law that vanishes for the maximum subcascade volume (described in [20, 21]). Comparison between MD and BCA cascades show a good agreement because the MD empirical potential has been adjusted on the ZBL potential used in BCA on the short distance range, that intervenes during the ballistic stage of the cascades. Notice that some atoms in MD cascades can experience channelling due to the crystal structure, and this is not accounted for in our BCA model. The channelling effect has been studied with other BCA codes that account for crystal structure, MARLOWE in [51] and MDRANGE compared to MD in [52]. Another difference is that in high energy MD cascades, small subcascades can disappear before the end of the ballistic stage. The BCA is still a convenient method to reach the number of trials necessary for good statistics, especially at high energy.

Subcascades can be seen as forming a multitype point pattern characterised by cross pair correlation functions. With no loss of generality we proposed to simplify the volume, which in principle evolves in continuous way, in discrete categories, reducing integrals into sums. The cross pair correlation functions exhibit a maximum because of the minimum distance required by the no overlap criterion and because the cascade is enclosed in a finite volume. Still the number of interacting pairs of subcascades is in principle given by the integral of the cross pair correlation function on a range of distance (and subcascade volume) but we consider that only close pairs are of interest. We propose a strong simplification taking the value of the cross pair correlation functions at their maximum multiplied by a thickness of 1 nm. We then studied the number of interacting pairs of subgroups i and j in cascade as a function of the PKA energies.

Cascade exhibiting branching are formed by elongated tracks decorated by small subcascades, which causes that the number of interactions of small subcascades increases proportionally to

the PKA energy. The number of medium (resp. large) subcascades pairs increases as square root of E (resp. $E^{1/4}$).

We included the number of interacting subcascades in our model of primary damage. In [20], a first term was determined for the defect cluster production in individual subcascades. Here pairwise terms have been added that correspond to the effect of subcascade interactions on the defect production. Three body terms could in principle be included and other mechanism of enhanced cluster formation cannot be excluded. Indeed, in [21], for example, we observed a change of the power law slope of defect cluster production in W cascades of energy smaller than the fragmentation energy. We proposed functional forms for the unknown features and ended up with a model with a limited number of parameters and physical meaning. Using our large database or MD cascades from [30], we directly compared and adjusted our model to the defects created in MD cascades. We showed that below the fragmentation energy, the defect production is correctly given by the first term of our model. The defect production of high energy cascade is not correctly predicted by the defect production in individual subcascades only. We explained and illustrated that this is due to the interaction of subcascades which increases the cluster fraction, i.e. the reduction of the frequency of small clusters and the enhanced formation of large ones. We observed that the subcascade interaction stabilizes large SIA clusters, resulting in fewer small ones, than with isolated subcascades without creating significantly more defects. We adjusted interaction functions, which permits the prediction of the primary damage of cascades whose energy is not accessible by full MD. More accurate results can be obtained by adjusting our model with more high energy cascades, or combining with other approaches to model the mechanism of these interactions. Further works are necessary to characterize the effect of subcascade interaction on vacancy clusters. We observed a correlation between the frequency of subcascade interactions and the enhanced formation of large clusters.

Still the physical mechanism must be clarified. It may be due to interaction of shock-waves as explained in [12]. Another possibility could be the migration of small interstitials that could be attracted or trapped in these regions. Other mechanisms could also impact the defect cluster production as the electronic losses and electron-phonon interaction. In this work, the cascade description along its main direction has not been taken into account. Indeed, in high energy ion irradiation, it is established that, the average damage distribution and the defect versus size frequency depends on the distance from the source (or surface) in the direction of the impinging particle. Also, the presence of a surface can change the frequency of clusters as described in [53]. Finally, though our model takes partially into account the electronic stopping power, it does not account for this specific heat transport and its effect on the defect recovery.

8. Conclusion

Using MD and BCA calculations we studied two morphological transitions of collision cascades in a large range of PKA energy. A first transition from compact to fragmented cascades is observed in all metals and the mean features depend on the atomic number and the atomic density. The fragmentation energy follows a simple power law of these two parameters. We introduced an energy criterion that improves the sensitivity of our method especially in high Z materials, and includes thermodynamic properties such as the melting point temperature.

The distribution of subcascade volumes and the spatial correlation of the subcascades can be accurately and efficiently studied using the BCA and statistics of random multitype point patterns. We derived the number of interacting subcascades as function of their volume described as a limited number of subgroups. We shown that a second transition exists when the cascade branching starts and the number of interacting small-small subcascades increases proportionally to the PKA energy while the number of medium (resp. large) subcascade pairs increases as square root of E (resp. $E^{1/4}$).

We developed our model of primary damage now including two terms: the production of defects in subcascades taken individually, and the pairwise terms of the subcascade interaction. The model has been applied to Fe. We have shown that the subcascade interaction increases the SIA cluster fraction in high energy cascades. It has been used to extrapolate the defect production for even larger PKA energy, but it could also be convoluted with the neutron PKA spectrum. Our approach is also valid for other metals or materials.

ORCID iDs

A De Backer ● https://orcid.org/0000-0003-2107-241X
A E Sand ● https://orcid.org/0000-0001-9041-1468
K Nordlund ● https://orcid.org/0000-0001-6244-1942

References

[1] Becquart C S, De Backer A and Domain C 2018 *Handbook of Mechanics of Materials: Atomistic Modeling of Radiation Damage in Metallic Alloys* ed C-H Hsueh *et al* (Berlin: Springer)

[2] Nordlund K H *et al* 2018 Improving atomic displacement and replacement calculations with physically realistic damage models *Nat. Commun.* **9** 1084

[3] Björkas C, Nordlund K and Caturla M J 2012 Influence of the picosecond defect distribution on damage accumulation in irradiated α-Fe *Phys. Rev.* B **85** 024105

[4] Adjanor G, Bugat S, Domain C and Barbu A 2010 Overview of the RPV-2 and intern-1 packages: from primary damage to microplasticity *J. Nucl. Mater.* **406** 175–86

[5] Gilbert M R, Sublet J-Ch and Dudarev S L 2017 Spatial heterogeneity of tungsten transmutation in a fusion device *Nucl. Fusion* **57** 044002

[6] Hou M 1989 Fuzzy clustering methods: an application to atomic displacement cascades in solids *Phys. Rev.* A **39** 2817–28

[7] Satoh Y, Kojima S, Yoshiie T and Kiritani M 1991 Criterion of subcascade formation in metals from atomic collision calculation *J. Nucl. Mater.* **179** 901–4

[8] Heinisch H L and Singh B N 1993 On the structure of irradiation-induced collision cascades in metals as a function of recoil energy and crystal structure *Phil. Mag.* A **67** 407–24

[9] Jumel S and Van-Duysen J C 2004 Incas: an analytical model to describe displacement cascades *J. Nucl. Mater.* **328** 151–64

[10] Ryazanov A I, Metelkin E V and Semenov E V 2009 Modeling of cascade and sub-cascade formation at high PKA energies in irradiated fusion structural materials *J. Nucl. Mater.* **386–8** 132–4 (*Fusion Reactor Materials Proc. of the Thirteenth Int. Conf. on Fusion Reactor Materials*)

[11] Lunéville L, Simeone D and Weber W J 2011 Study of the fragmentation of a displacement cascade into subcascades within the binary collision approximation framework *J. Nucl. Mater.* **415** 55–60

[12] Calder A F, Bacon D J, Barashev A V and Osetsky Yu N 2010 On the origin of large interstitial clusters in displacement cascades *Phil. Mag.* **90** 863–84

[13] Setyawan W, Selby A P, Juslin N, Stoller R S, Wirth B D and Kurtz R J 2015 Cascade morphology transition in bcc metals *J. Phys.: Condens. Matter* **27** 225402

[14] Crocombette J-P and Jourdan T 2015 Cell molecular dynamics for cascades (CMDC): a new tool for cascade simulation *Nucl. Instrum. Methods Phys. Res.* B **352** 9–13 (*Proc. of the 12th Int. Conf. on Computer Simulation of Radiation Effects in Solids (Alacant, Spain, 8–13 June 2014)*)

[15] Crocombette J-P, Van Brutzel L, Simeone D and Luneville L 2016 Molecular dynamics simulations of high energy cascade in ordered alloys: defect production and subcascade division *J. Nucl. Mater.* **474** 134–42

[16] Jourdan T and Crocombette J-P 2018 On the transfer of cascades from primary damage codes to rate equation cluster dynamics and its relation to experiments *Comput. Mater. Sci.* **145** 235–43

[17] Lunéville L, Simeone D and Jouanne C 2006 Calculation of radiation damage induced by neutrons in compound materials *J. Nucl. Mater.* **353** 89–100

[18] Sand A E, Dudarev S L and Nordlund K 2013 High energy collision cascades in tungsten: dislocation loops structure and clustering scaling laws *Eur. Phys. Lett.* **103** 46003

[19] Sand A E, Aliaga M J, Caturla M J and Nordlund K 2016 Surface effects and statistical laws of defects in primary radiation damage: tungsten versus iron *Europhys. Lett.* **115** 36001

[20] De Backer A, Sand A E, Nordlund K, Lunéville L, Simeone D and Dudarev S L 2016 Subcascade formation and defect cluster size scaling in high-energy collision events in metals *Europhys. Lett.* **115** 26001

[21] Sand A E, Mason D R, De Backer A, Yi X, Dudarev S L and Nordlund K 2017 Cascade fragmentation: deviation from power law in primary radiation damage *Mater. Res. Lett.* **5** 1–7

[22] Yi X, Sand A E, Mason D R, Kirk M A, Roberts S G, Nordlund K and Dudarev S L 2015 Direct observation of size scaling and elastic interaction between nano-scale defects in collision cascades *Europhys. Lett.* **110** 36001

[23] Eckstein W, Mutzke A, Schneider R and Dohmen R 2011 SDTrimSP version 5.00 *IPP Report12/08* MaxPlanck-Institut fr Plasmaphysik

[24] Eckstein W 1991 *Computer Simulation of Ion-Solid Interactions* vol 10 (Berlin: Springer)

[25] Ziegler J F, Biersack J P and Littmark U 1985 *The Stopping and Range of Ions in Matter* (New York: Pergamon)

[26] Ziegler J F, Ziegler M D and Biersack J P 2010 SRIM—The stopping and range of ions in matter (2010) *Nucl. Instrum. Methods Phys. Res.* B **268** 1818–23

[27] Oen O S and Robinson M T 1976 Computer studies of the reflection of light ions from solids *Nucl. Instrum. Methods* **132** 647–53

[28] Zarkadoula E, Daraszewicz S L, Duffy D M, Seaton M, Todorov I T, Nordlund K, Dove M T and Trachenko K 2014 Electronic effects in high-energy radiation damage in iron *J. Phys.: Condens. Matter* **26** 085401

[29] Zarkadoula E, Duffy D M, Nordlund K, Seaton M A, Todorov I T, Weber W J and Trachenko K 2015 Electronic effects in high-energy radiation damage in tungsten *J. Phys.: Condens. Matter* **27** 135401

[30] Domain C, De Backer A and Becquart C S 2018 in preparation

[31] Becquart C S, Decker K M, Domain C, Ruste J, Souffez Y, Turbatte J C and Van Duysen J C 1997 Massively parallel molecular dynamics simulations with EAM potentials *Radiat. Eff. Defects Solids* **142** 9–21

[32] Ackland G J, Mendelev M I, Srolovitz D J, Han S and Barashev A V 2004 Development of an interatomic potential for phosphorus impurities in α-iron *J. Phys.: Condens. Matter* **16** S2629

[33] Olsson P, Becquart C S and Domain C 2016 *Ab initio* threshold displacement energies in iron *Mater. Res. Lett.* **4** 219–25

[34] Stoller R E, Odette G R and Wirth B D 1997 Primary damage formation in bcc iron *J. Nucl. Mater.* **251** 49 (*Proc. of the Int. Workshop on Defect Production, Accumulation and Materials Performance in an Irradiation Environment*)

[35] Granato A V 1992 Interstitial model for condensed matter states of face-centered-cubic metals *Phys. Rev. Lett.* **68** 974

[36] Nordlund K and Averback R S 1998 The role of self-interstitial atoms on the high temperature properties of metals *Phys. Rev. Lett.* **80** 4201–4

[37] Nordlund K, Ashkenazy Y, Averback R S and Granato A V 2005 Strings and interstitials in liquids, glasses and crystals *Europhys. Lett.* **71** 625

[38] Forsblom M and Grimvall G 2005 Homogeneous melting of superheated crystals: molecular dynamics simulations *Phys. Rev.* B **72** 054107

[39] White G K and Collocott S J 1984 Heat capacity of reference materials: Cu and W *J. Phys. Chem. Ref. Data* **13** 1251–7

[40] Olsson P, Klaver T P C and Domain C 2010 *Ab initio* study of solute transition-metal interactions with point defects in bcc Fe *Phys. Rev.* B **81** 054102

[41] Simeone D, Lunéville L and Serruys Y 2010 Cascade fragmentation under ion beam irradiation: a fractal approach *Phys. Rev.* E **82** 011122

[42] Robinson M T and Torrens I M 1974 Computer simulation of atomic-displacement cascades in solids in the binary-collision approximation *Phys. Rev.* B **9** 5008–24

[43] Micoulaut M 2004 Structure of densified amorphous germanium dioxide *J. Phys.: Condens. Matter* **16** L131

[44] Marrocchelli D, Salanne M and Madden P A 2010 High-pressure behaviour of GeO$_2$: a simulation study *J. Phys.: Condens. Matter* **22** 152102

[45] Philippe T, Duguay S, Grancher G and Blavette D 2013 Point process statistics in atom probe tomography *Ultramicroscopy* **132** 114–20 (*IFES 2012*)

[46] Wiegand T and Moloney K A 2013 *Handbook of Spatial Point-Pattern Analysis in Ecology* (London: Chapman and Hall)

[47] Illian J, Penttinen A, Stoyan H and Stoyan D 2008 *Statistical Analysis and Modelling of Spatial Point Patterns* (New York: Wiley)

[48] Gelfand A E, Diggle P J, Fuentes M and Guttorp P 2010 *Handbook of Spatial Statistics* (Boca Raton, FL: CRC Press)

[49] Bacon D J, Calder A F and Gao F 1997 Defect production due to displacement cascades in metals as revealed by computer simulation *J. Nucl. Mater.* **251** 1–12 (*Proc. of the Int. Workshop on Defect Production, Accumulation and Materials Performance in an Irradiation Environment*)

[50] Baudin M, Dutfoy A, Iooss B and Popelin A-L 2017 Openturns: an industrial software for uncertainty quantification in simulation *Handbook of Uncertainty Quantifications* (Berlin: Springer) pp 2001–38

[51] Hou M, Ortiz C J, Becquart C S, Domain C, Sarkar U and De Backer A 2010 Microstructure evolution of irradiated tungsten: crystal effects in He and H implantation as modelled in the binary collision approximation *J. Nucl. Mater.* **403** 89–100

[52] Nordlund K, Djurabekova F and Hobler G 2016 Large fraction of crystal directions leads to ion channeling *Phys. Rev.* B **94** 214109

[53] Aliaga M J, Schäublin R, Löffler J F and Caturla M J 2015 Surface-induced vacancy loops and damage dispersion in irradiated fe thin films *Acta Mater.* **101** 22–30